Lunar pickup ions observed by ARTEMIS: Spatial and temporal distribution and constraints on species and source locations

J. S. Halekas,[1,2] A. R. Poppe,[1,2] G. T. Delory,[1,2] M. Sarantos,[2,3,4] W. M. Farrell,[2,3] V. Angelopoulos,[5] and J. P. McFadden[1]

Received 20 April 2012; revised 14 May 2012; accepted 15 May 2012; published 30 June 2012.

[1] ARTEMIS observes pickup ions around the Moon, at distances of up to 20,000 km from the surface. The observed ions form a plume with a narrow spatial and angular extent, generally seen in a single energy/angle bin of the ESA instrument. Though ARTEMIS has no mass resolution capability, we can utilize the analytically describable characteristics of pickup ion trajectories to constrain the possible ion masses that can reach the spacecraft at the observation location in the correct energy/angle bin. We find that most of the observations are consistent with a mass range of ~20–45 amu, with a smaller fraction consistent with higher masses, and very few consistent with masses below ~15 amu. With the assumption that the highest fluxes of pickup ions come from near the surface, the observations favor mass ranges of ~20–24 and ~36–40 amu. Although many of the observations have properties consistent with a surface or near-surface release of ions, some do not, suggesting that at least some of the observed ions have an exospheric source. Of all the proposed sources for ions and neutrals about the Moon, the pickup ion flux measured by ARTEMIS correlates best with the solar wind proton flux, indicating that sputtering plays a key role in either directly producing ions from the surface, or producing neutrals that subsequently become ionized.

Citation: Halekas, J. S., A. R. Poppe, G. T. Delory, M. Sarantos, W. M. Farrell, V. Angelopoulos, and J. P. McFadden (2012), Lunar pickup ions observed by ARTEMIS: Spatial and temporal distribution and constraints on species and source locations, *J. Geophys. Res.*, *117*, E06006, doi:10.1029/2012JE004107.

1. Introduction

[2] Despite the seeming simplicity of the Moon-solar wind interaction, the lunar environment has a rich array of diverse and interesting physical processes, many resulting from the direct bombardment of the lunar surface by charged particles and other impactors such as micrometeorites and solar photons [*Halekas et al.*, 2011]. Ions of lunar origin represent one such phenomenon with linkages between the surface, the plasma, the neutral exosphere, and all of these external drivers. Lunar ions originate from solar wind sputtering from the surface, and from ionization and dissociation of neutral exospheric gases, which themselves are released by charged particle and photon sputtering, micrometeorite impact, thermal desorption, and volatile release from the interior, among other processes [*Stern*, 1999]. Therefore, by measuring pickup ions around the Moon, we can gain knowledge about all of these fundamental physical processes, and tie charged particle data back to the lunar surface and exosphere.

[3] We still have a relatively poor inventory of the species that comprise the tenuous lunar exosphere. As summarized in Table 1, we know from a combination of ALSEP surface measurements [*Hoffman et al.*, 1973; *Hoffman and Hodges*, 1975; *Freeman and Benson*, 1977] and remote spectroscopy [*Fastie et al.*, 1973; *Feldman and Morrison*, 1991; *Flynn and Stern*, 1996; *Stern et al.*, 1997; *Potter and Morgan*, 1988; *Mendillo et al.*, 1991] that the most abundant species positively detected so far in the exosphere are He and Ar. On the other hand, the species we know most about, the alkalis Na and K, have small near-surface densities. The number of ions produced from each exospheric species depends on their neutral density and their scale height (together giving the column density) as well as the total ionization rate of that species (Table 1 summarizes photo-ionization rates, which usually dominate over charge exchange and electron impact ionization). The scale height (or scale heights, if multiple processes operate) depends on particle mass and on the process-dependent starting energy distribution for released gases, and is not well known for many species. The total neutral column density for the alkalis Na and K, which have large

[1]Space Sciences Laboratory, University of California, Berkeley, California, USA.
[2]NASA's Lunar Science Institute, NASA Ames Research Center, Moffett Field, California, USA.
[3]Heliophysics Science Division, NASA Goddard Space Flight Center, Greenbelt, Maryland, USA.
[4]Goddard Planetary Heliophysics Institute, University of Maryland, Baltimore County, Baltimore, Maryland, USA.
[5]Department of Earth and Space Sciences, University of California, Los Angeles, California, USA.

Corresponding author: J. S. Halekas, Space Sciences Laboratory, 7 Gauss Way, University of California, Berkeley, CA 94720, USA. (jazzman@ssl.berkeley.edu)

0148-0227/12/2012JE004107

Table 1. Expected Lunar Pickup Ion Species[a]

	Neutral Density (cm^{-3})	Photo Rate Coefficient (s^{-1})	Sputter Yield
Mass 1 (H^+)	<17	7.3×10^{-8}	
Mass 2 (H_2^+)	<9000	5.4×10^{-8}	
Mass 4 (He^+)	2000	5.3×10^{-8}	
Mass 12 (C^+)	<200	4×10^{-6}	
Mass 14 (N^+)	<600	1.9×10^{-7}	
Mass 16 (O^+)	<500	2×10^{-7}	
Mass 16 (CH_4^+)	<10,000	3.6×10^{-7}	
Mass 17 (OH^+)	$<1 \times 10^6$	2.4×10^{-7}	
Mass 23 (Na^+)	70	1.6×10^{-5}	7×10^{-6}
Mass 24 (Mg^+)	<6000		9×10^{-6}
Mass 27 (Al^+)	<55		1.5×10^{-5}
Mass 28 (Si^+)	<48		6×10^{-6}
Mass 28 (N_2^+)	800	3.5×10^{-7}	
Mass 29 (CO^+)	<1000	4×10^{-7}	
Mass 39 (K^+)	17	2×10^{-5}	3×10^{-6}
Mass 40 (Ca^+)	<1		2×10^{-6}
Mass 40 (Ar^+)	100,000	3×10^{-7}	
Mass 44 (CO_2^+)	<1000	6.5×10^{-7}	
Mass 56 (Fe^+)	<380		3×10^{-6}

[a]Dayside neutral densities after *Stern* [1999] with values from *Feldman and Morrison* [1991], *Hoffman and Hodges* [1975], *Hoffman et al.* [1973], *Potter and Morgan* [1988], *Fastie et al.* [1973], *Stern et al.* [1997], and *Flynn and Stern* [1996]. Quiet sun photo-ionization rates are from *Huebner et al.* [1992], and sputter yields are from *Elphic et al.* [1991].

scale heights [*Potter and Morgan*, 1988; *Stern and Flynn*, 1995], may in fact compare to that of many other species more abundant in the lunar regolithy, especially if photo-stimulated desorption plays an important role [*Sarantos et al.*, 2010, 2012]. In that case, given their very large photo-ionization rates, we should expect substantial fluxes of Na^+ and K^+ ions around the Moon.

[4] Charged particle sputtering from the surface also directly releases some ions, therefore producing pickup ions without the intermediate stages of residence in the exosphere and subsequent ionization. Much of our knowledge of this process comes from a laboratory experiment by *Elphic et al.* [1991]. Charged particle sputtering of lunar elements mainly releases ions with low ionization energies, such as Al^+, Si^+, and Mg^+ (see Table 1 for sputter yields from lunar materials). The number of ions produced by sputtering depends directly on the flux of incoming ions, and, to a degree, on their mass and energy distribution, which can have important implications during major solar events [*Killen et al.*, 2012]. The relative contributions to pickup ion fluxes from surface sputtering and photo-ionization depend on ion species, but could have similar magnitudes in some cases [*Yokota and Saito*, 2005].

[5] Once born (ionized), ions feel the effect of electric and magnetic fields in the ambient plasma. Depending on the electric field, these ions either re-impact the surface or follow cycloidal trajectories extending downstream in the plane of the electric field, with the scale and bend-back of the cycloid depending on ion species. These pickup ions provide a useful tool to study the lunar surface and exosphere [*Hartle and Killen*, 2006]. Ions observed near the Moon span a wide variety of species, with mass 20–28 and 40–44 atomic mass units (amu) seen at the surface by the ALSEP SIDE instrument [*Freeman and Benson*, 1977; *Vondrak et al.*, 1974], H_2^+, He^+, C^+, O^+, Na^+, and K^+ reported at ~100 km by Kaguya and Chang'E [*Yokota et al.*, 2009; *Tanaka et al.*, 2009; *Wang et al.*, 2011], and O^+, Al^+, and Si^+ identified at greater distances by AMPTE and Wind [*Cladis et al.*, 1994; *Hilchenbach et al.*, 1991, 1993; *Mall et al.*, 1998]. Many of these species correspond to basic expectations, given the estimated neutral abundances, photo-ionization rates, and sputter yields shown in Table 1, while some do not. In particular, the significant fluxes of O^+ and C^+ observed at high altitudes by previous missions appear somewhat unexpected, given their low neutral abundances [*Feldman and Morrison*, 1991] and low expected sputtering yields [*Elphic et al.*, 1991]. Some of these ions could result from photo-dissociation of molecular species [*Hoffman and Hodges*, 1975; *Hodges*, 1976].

2. ARTEMIS Observations of Lunar Pickup Ions

[6] The two-probe ARTEMIS (Acceleration, Reconnection, Turbulence, and Electrodynamics of Moon's Interaction with the Sun) mission [*Angelopoulos*, 2011] repurposed two spacecraft from the original five-probe THEMIS constellation on an extended mission to the Moon. The two ARTEMIS probes, which entered lunar orbit in June and July of 2011 in highly elliptical equatorial orbits, provide comprehensive plasma measurements, including three-dimensional ion flux measurements from the ESA instrument [*McFadden et al.*, 2008a] and 3-axis magnetic field measurements from the MAG instrument [*Auster et al.*, 2008]. In mid-September 2011, the ESA instruments were put into magnetospheric mode near the Moon [*McFadden et al.*, 2008a], allowing observation of pickup ions. In magnetospheric mode, the ESA instruments measure an energy range extending up to ~25 keV with full angular coverage, with ~30% energy resolution and 22.5° resolution. Unfortunately, the ESA instrument has no mass-resolving capabilities, so we must infer the species of pickup ions from other characteristics of the observation.

[7] Figure 1 shows a simultaneous pickup ion observation by ARTEMIS probes P1 and P2, and Figure 2 shows the orbits and field geometry for this observation. This event illustrates the defining characteristics of all ARTEMIS pickup ion observations considered in this paper. Given plasma (e.g., the solar wind) with a magnetic field **B** flowing past the Moon with velocity **U**, a convection electric field $\mathbf{E} = -\mathbf{U} \times \mathbf{B}$ exists in the Moon frame. Pickup ions respond to **E** and **B**, accelerating along the electric field **E** from their production point and subsequently following cycloidal trajectories in the plane containing the electric field **E** and the solar wind velocity **U** and perpendicular to **B**. For ARTEMIS to easily observe these ions their trajectories must lie close to the nearly equatorial (XY) plane of the probe orbits; therefore **B** must have a dominant +/−Z-component, and **E** a correspondingly dominant +/−Y-component. Since pickup ion trajectories bend back from the *y* axis, ARTEMIS usually observes these ions in their first gyroorbit at large +/−Y and somewhat negative X coordinates. The pickup ions form a highly collimated beam, generally producing a signal in only a single energy-angle bin of the ESA instrument. At a few times, ions span multiple energy bins, indicating either an extended source of pickup ions, fluctuations in the fields during the ESA integration period, or simply an ion energy falling near the boundary between two energy bins.

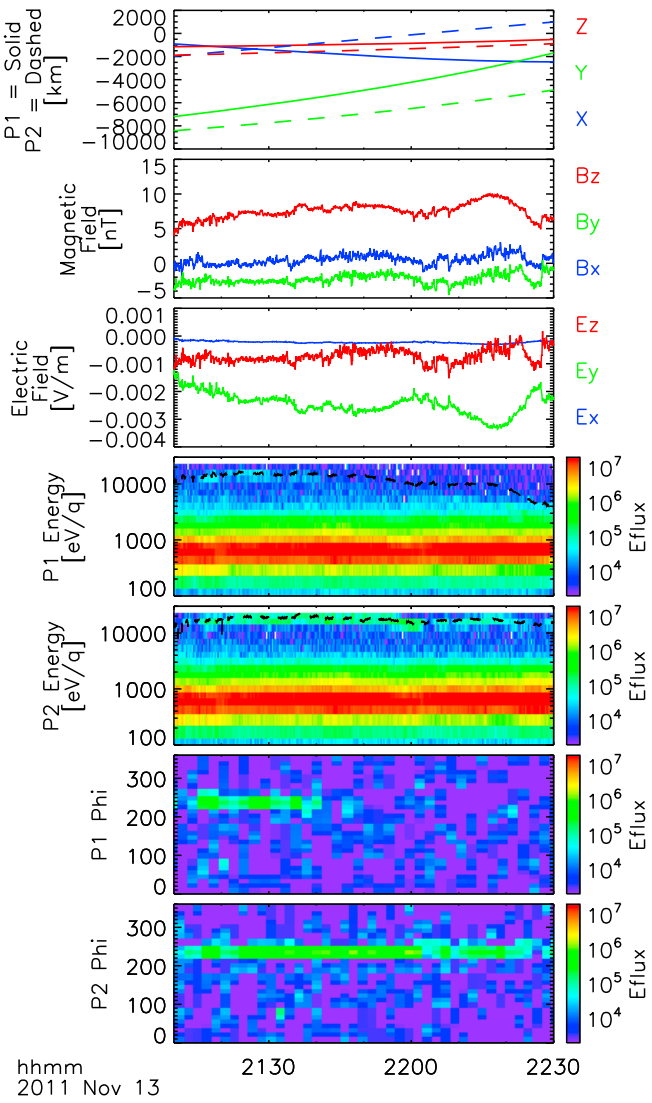

Figure 1. A simultaneous pickup ion observation by both ARTEMIS probes, showing spacecraft position, magnetic field, derived convection electric field, and ion differential energy flux [eV/(cm^2 s sr eV)] for P1 and P2 as a function of energy and phi angle (for 10–25 keV ions) in the equatorial plane. Dashed black lines on energy spectra show kinetic energy gained from electric field for ions born at the sub-solar point. All vector quantities use SSE (Selenocentric Solar Ecliptic) coordinates.

[8] The kinetic energy per charge W/q gained by a pickup ion depends only on the electric field **E** and the distance traveled from the source along that field. The quantity $\Delta W/q = \int \vec{E}\cdot d\vec{r}$ is shown on the energy spectra in Figure 1 for a source location at the sub-solar point. The energy per charge of the observed beam matches that expected for pickup ions coming from near the Moon, supporting our identification. Unfortunately, since this quantity does not depend on mass, it alone does not help to identify the species of the ions.

[9] The characteristic radius of the ion trajectory, however, and thus the degree to which it bends as the ion travels out from the Moon, depends on the ion's mass. As a result, at large lateral distances only higher mass ions can reach the spacecraft from near the surface. A pickup ion follows a trajectory with a drift velocity of $(\mathbf{E}\times\mathbf{B})/B^2$ (or equivalently $\mathbf{U_{perp}}$, the component of the plasma flow velocity perpendicular to the magnetic field). Pickup ion trajectories have a cycloidal form, scaling with the ion gyroradius $R_M = Mm_PU_{perp}/(qB) = MR_P$ (where M is ion mass number and m_P and R_P are the mass and perpendicular gyroradius of a solar wind proton), and lie in the plane of **E** and **U**, with maximum displacement relative to the drift vector of $2R_M$ (or $2MR_P$) in the direction of **E**. For the flow speeds of ~320 km/s and the magnetic fields of ~7 nT during this event, R_P = ~500 km. Therefore, the lateral distance of 4,000–6,000 km from the lunar surface indicates that no pickup ions with M < 4–6 can reach the spacecraft from near the surface on this occasion. We will see that the observed

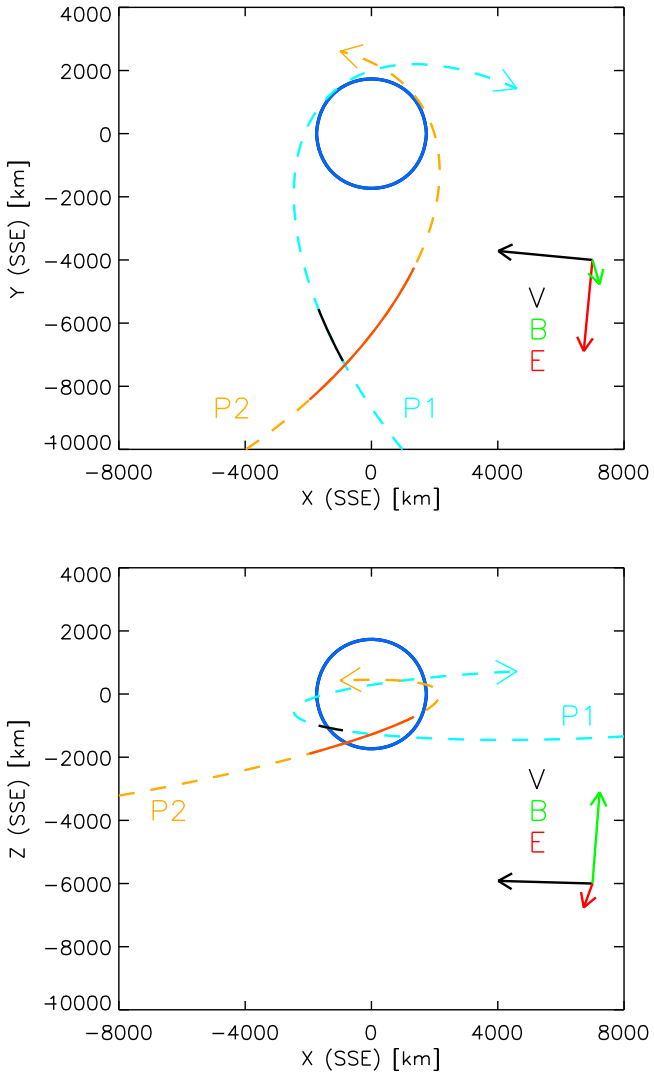

Figure 2. ARTEMIS P1 and P2 orbits for the even shown in Figure 1, in dashed blue and dashed orange respectively. The black and solid dark orange sections show the locations of pickup ions seen by P1 and P2 respectively. Black, green, and red vectors show the solar wind velocity, the interplanetary magnetic field, and the convection electric field derived from these two quantities.

pickup ion velocity angles provide a more stringent constraint, since they indicate that the observed pickup ions have not yet reached the peak of their cycloidal motion.

[10] Meanwhile, a proton reflected from the surface [*Saito et al.*, 2008] or from a magnetic anomaly [*Lue et al.*, 2011], which can have a starting energy as large as that of the incident solar wind protons, can reach a lateral distance of at most $4R_P$ (for reflection in the opposite direction from the solar wind, and thus the largest possible starting velocity in the solar wind frame). Therefore, no reflected solar wind protons can reach the spacecraft from near the surface at this time. This is an important conclusion, since reflected protons can dominate over pickup ions near the Moon.

[11] At both P1 and P2, an integration over the distribution function of the pickup ion plume gives a total density estimate varying from (0.002–.005)*$\sqrt{M}$ cm^{-3} over the course of the event, with M the unknown ion atomic mass (see *McFadden et al.* [2008b] for the correct mass-scaling of the density moment calculation). This density is quite large compared to the peak exospheric pickup ion densities of 5×10^{-4} for He^+ and 3×10^{-3} for Na^+ estimated by *Hartle et al.* [2011], suggesting a contribution by multiple ion species, the existence of conditions much more favorable for exospheric pickup ion production than assumed by these authors, or a substantial contribution from direct surface sputtering.

3. Constraining Lunar Pickup Ion Species

[12] Three challenges face us in using ARTEMIS observations to identify lunar pickup ions. First and foremost, the ESA instrument does not measure mass composition directly. Furthermore, the instrument does not have a delta function response in energy or angle. Finally, the Moon does not provide a delta-function source. All of these factors prevent the direct identification of pickup ion species. However, by utilizing the fact that pickup ions originate at or near the lunar surface, with zero energy (to a very good approximation), we can partially overcome these challenges.

[13] As described in Section 2, pickup ions follow easily analytically described cycloidal trajectories, starting with zero velocity and reaching a known peak velocity (twice the drift velocity) at the top of the cycloid. Therefore, we will observe pickup ions with a precise relationship between gyrophase and kinetic energy that depends ion mass. We can parameterize a pickup ion trajectory in uniform magnetic and electric fields as [$X_P = X_{P0} + R_M*(\theta - \sin(\theta))$, $Y_P = Y_{P0} + R_M*(1-\cos(\theta))$], where [$X_P$,$Y_P$] are coordinates aligned with the drift velocity $\mathbf{U_{perp}}$ and the electric field $\mathbf{E}$ respectively, and θ represents the gyrophase. The pickup ion energy per charge W/q is simply $E*(Y_P - Y_{P0})$. Hence, the relationships between the energy of an ion and its arrival direction for a given mass and starting location allow us to constrain the species of observed ions. Given knowledge of the fields, we can therefore analytically construct possible trajectories for each ion species to determine which ions have trajectories that can reach the spacecraft at the observation point and in the correct energy/angle bin, thereby constraining the most likely mass range for observed ions, at each observation time.

[14] In everything that follows, we use direct ARTEMIS ESA and MAG measurements of $\mathbf{U}$ and $\mathbf{B}$ and derive $\mathbf{E} = -\mathbf{U} \times \mathbf{B}$ from these quantities. Since the ESA does not resolve the off-axis components of the solar wind velocity well in magnetospheric mode, we use the known aberration velocity of ~30 km/s associated with the Earth's orbit around the Sun, and assume no other off-axis flow components. We have tested with various assumptions and found that the small off-axis components expected in the solar wind do not significantly affect any of our results. Even near the edge of the magnetosheath, where the event of Figures 1–2 took place, off-axis components did not reach significant enough levels to alter our results.

[15] Our analytic trajectory calculation implicitly assumes steady fields over the travel time of the pickup ions. We typically observe pickup ions with a gyrophase on the order of ~60°, corresponding to a travel time of $1/(6*f_{ci}) = 2\pi M m_P/(6qB)$, which works out to a few seconds for light ions and up to a minute for heavier ions under typical conditions. Although some small-scale solar wind field fluctuations exist on a time scale shorter than this, corresponding to some minor perturbation of pickup ion trajectories, large scale fields generally remain steady for much longer time periods during the events we have considered, allowing us to assume constant external conditions to a reasonably good approximation.

[16] The ESA has an intrinsic energy resolution of ~18% and an intrinsic angular resolution of ~7° and 5°−22.5° in phi and theta. However, in magnetospheric mode, the processor sums multiple energy/angle bins onboard while creating the full 3-d distributions, resulting in a roughly Gaussian energy response with a FWHM of ~30%, a somewhat double-peaked phi response with total width of 22.5°, and a nearly square theta response with a width of 22.5°. Therefore, ions measured in a given energy/angle bin could in principle have landed anywhere in a 22.5° × 22.5° angular bin and within an ~30% FWHM energy window. For each possible ion mass, we can identify a bundle of trajectories consistent with these response functions.

[17] We show a sample of the resulting trajectories for a range of masses for one observation during our example event in Figure 3, for both P1 and P2. For each assumed ion mass, the range of allowed energy and angle for a single ESA bin corresponds to a line of ion production points lying in the plane perpendicular to $\mathbf{B}$ that passes through the spacecraft. It may seem surprising that these points form a line, rather than a more extended region, but this simply reflects the mathematical relationship between energy and gyrophase for a pickup ion that passes through a given observation point, which removes a degree of freedom for the starting locations. These production points correspond to trajectories that reach the spacecraft in the observed energy bin, but with energies corresponding to a range of ESA sensitivities, with the peak energy response corresponding to the central part of the production line, as seen in Figure 3. We find that no ions with mass below ~20 amu can reach either spacecraft with the correct energy and angle, given their smaller bend radius. For P1, no real pickup ions with a mass greater than ~40 amu can reach the spacecraft, since their trajectories would have had to start below the surface. For P2, on the other hand, inferred trajectories start farther from the surface, and a much wider range of ion species could reach the spacecraft in the correct energy/angle bin.

[18] We show the resulting constraints on pickup ion species and source altitude for this observation time as a

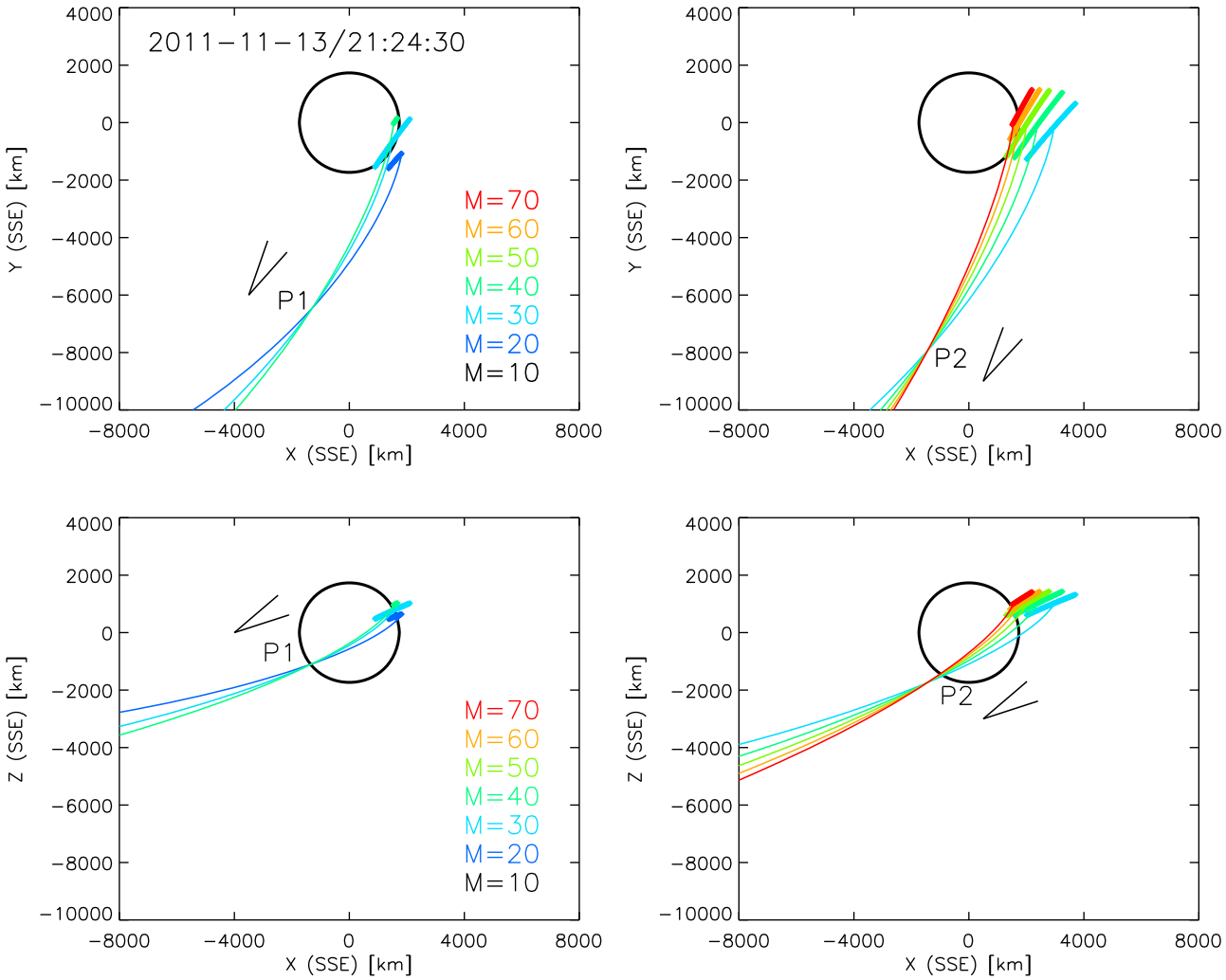

Figure 3. Pickup ion trajectories that could reach the two ARTEMIS probes ((left) P1; (right) P2) in the correct energy/angle bin and at the correct location at one time during the event of Figures 1 and 2, for a range of ion masses. For each mass, the trajectory shown corresponds to the peak of the energy response for the bin in which pickup ions were seen. Other points indicate the starting locations of other trajectories that could reach the spacecraft in the correct energy/angle bin. Black v-shapes outline the angular response of the ESA angle bin in which pickup ions were seen, for each probe.

function of ion mass in Figure 4. As seen above, only ions in the mass range of ∼20–40 amu can reach P1 in the correct energy/angle bin, whereas any mass > ∼25 amu can reach P2 in the correct bin, albeit with rather large starting altitudes for some of these possible masses. The P2 starting locations do not overlap with those for P1 for any mass, suggesting an extended source of ions and/or multiple ion species at this time. We can already reach some tentative but interesting conclusions from the mass/altitude constraints for this single observation. The mass range 20–40 amu, agreeing with the range of 23–37 amu inferred indirectly by AMPTE [*Hilchenbach et al.*, 1993], contains several interesting species (see Table 1). The molecular ions N_2^+ and CO^+ have not been previously reported, and have relatively low photo-ionization rates, so appear unlikely candidates. The alkali metals Na^+ and K^+, which make good physical sense given their high sputtering yields and photo-ionization rates, agree with lower-altitude measurements from Kaguya [*Yokota et al.*, 2009; *Tanaka et al.*, 2009]. Mg, Al, and Si also have respectable sputtering yields of ions, and agree with more distant Wind observations [*Mall et al.*, 1998]. The average inferred starting altitude for P2 lies well above the lunar surface, more consistent with exospheric sources, leading us to a tentative preference for photo-ionized exospheric Na and K for this event and potentially providing an exciting link to earth-based observations.

4. Spatial Distribution of Lunar Pickup Ion Observations

[19] We collected a data set of ARTEMIS pickup ion observations during the time range of 9/15/ 2011–2/5/2012 by visually searching all measured ion energy spectra for narrow features with energy per charge well separated from the solar wind proton and alpha particle populations, and picking out the energy/angle bin with the peak pickup ion flux from each corresponding 3-d ion distribution. In practice, we can easily pick out such features for any values

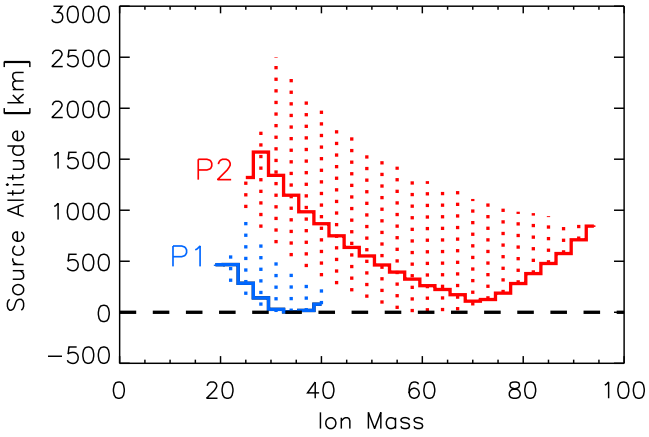

Figure 4. The range of allowed ion masses and starting altitudes for the time shown in Figure 3, for each of the two ARTEMIS probes. Solid lines indicate trajectories corresponding to the peak energy response for the bin in which pickup ions were seen, or to the highest response for an allowed trajectory, for cases where the peak response does not correspond to an allowed trajectory. Dotted vertical lines show the range of starting altitudes for all trajectories with the given mass that could reach the spacecraft in the correct energy/angle bin at the correct location.

above ~4–5 times the solar wind energy per charge. However, in the end, we reject many low-energy observations due to possible contamination by reflected protons. To remove reflected proton contamination, we reject observations that lie less than $4R_P$ in lateral distance (along the electric field direction) from the lunar surface. This definitively removes any observations contaminated by reflected protons, but also effectively prevents us from observing H_2^+ from any location near the Moon, since H_2^+ reaches a maximum lateral distance of $2R_M(H_2) = 4R_P$ from its source.

[20] In principle, we can observe ions (for at least some range of gyrophases) for any ion mass greater than 2. However, two effects make it somewhat less likely for us to see very low-mass ions, in particular He^+. First, removing proton contamination erodes our sensitivity to the lowest-mass ions, since we cannot observe them at low gyrophases (low gyrophases map to small distances from the Moon, especially for low-mass ions). In addition, for species that have a neutral scale height comparable to the size of their trajectories (usually, the lowest-mass ions), we may not observe a beam as sharply peaked in energy, making it more difficult to visually identify pickup ions. The lateral scale size of the source region that produces trajectories observable at a given location is at most a few times the scale height for a given species (see Figure 3, for example). If this lateral scale is not small compared to the distance to the observation location, or equivalently if the energy width of the feature is not small compared to the average observed pickup ion energy, we cannot as easily pick out a narrow pickup ion feature in the energy spectrum.

[21] For He^+, which has a scale height of ~1000 km [*Stern*, 1999], the energy width could reach ~2–4 kV for typical conditions ($W/q = E^*(Y_P - Y_{P0})$, and E ~2 mV/m in the solar wind). As a result, we will only reliably pick out a narrow He^+ feature in the energy spectra if it has a center energy on the order of ~8 kV or greater. He^+ ions reach this energy for a portion of their orbits near the peak of their

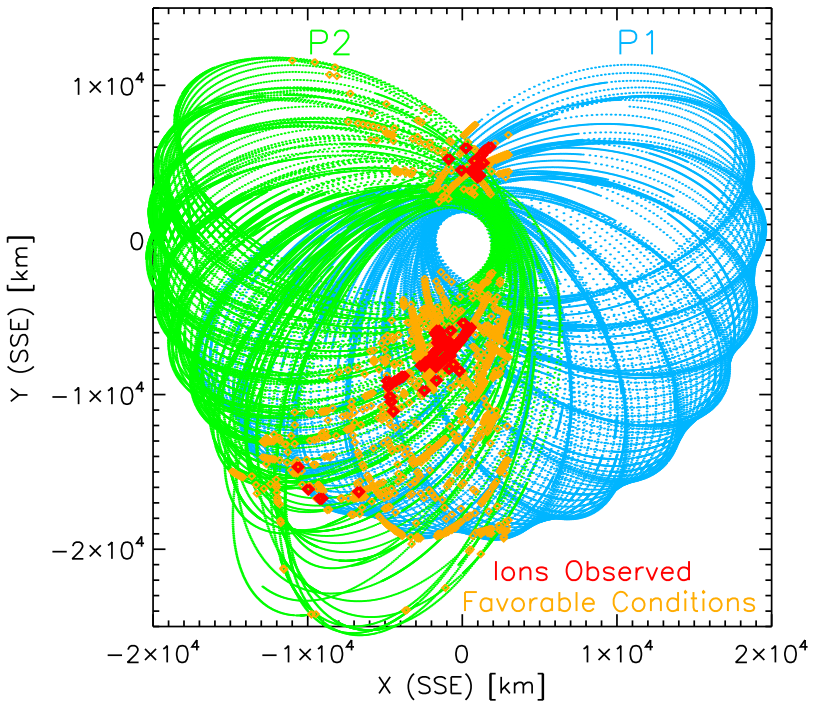

Figure 5. ARTEMIS orbits from September 15th, 2011 through February 5th, 2012, for P1 in blue and P2 in green. Orange points indicate times and locations with conditions favorable for observation of pickup ions by one of the probes (as described in text). Red points indicate times and locations where one of the ARTEMIS probes actually observed pickup ions.

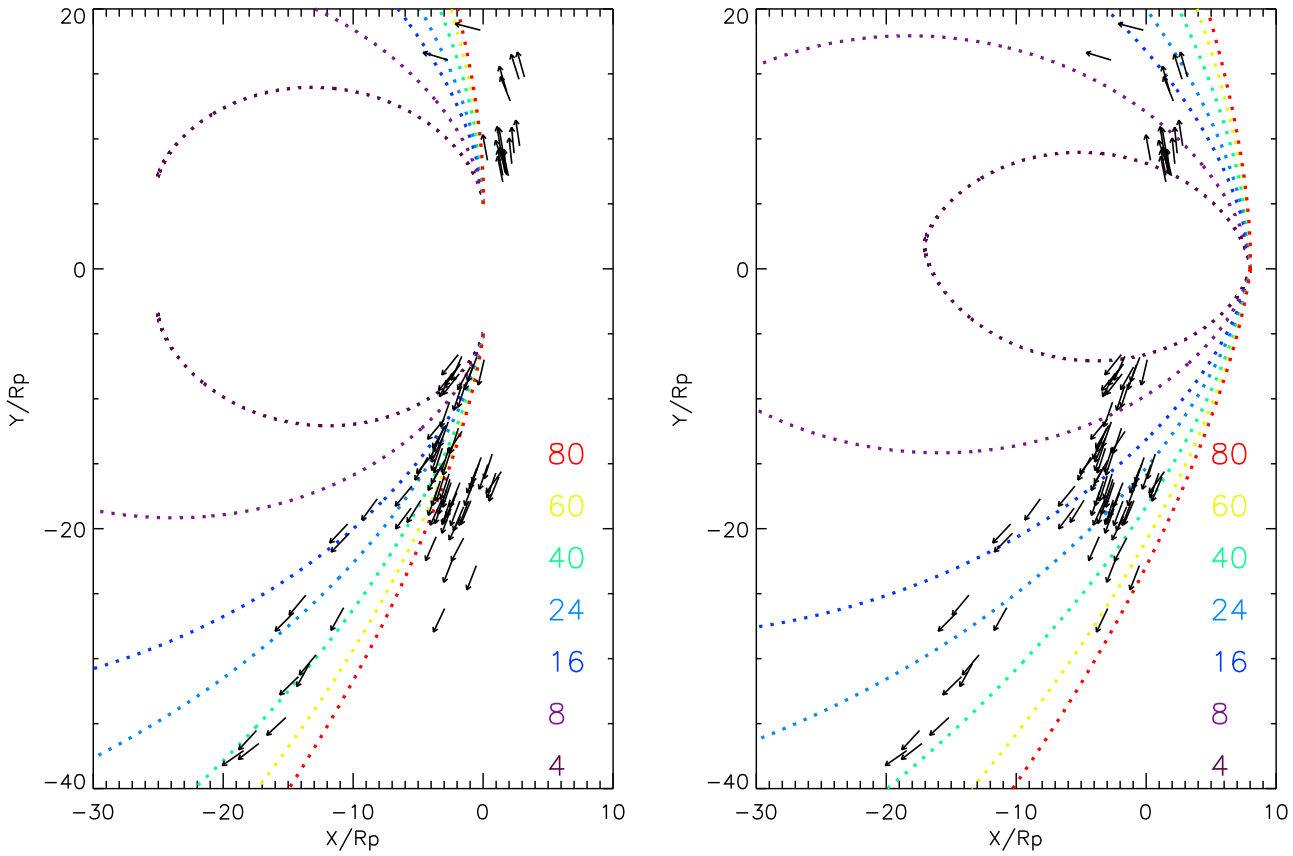

Figure 6. Locations and trajectories of 100 pickup ion plumes observed by both ARTEMIS probes during the time period of Figure 5, in coordinates normalized by the gyroradius of a solar wind proton R_P for each observation. Colored dashed curves show a range of sample trajectories for different ion masses, for start points above the (left) terminator and (right) sub-solar point, for electric fields pointing in the +Y and –Y directions.

cycloidal motion, under typical conditions. Therefore, on average, we will tend to have lower (but nonzero) sensitivity to He^+ than to heavier ions. A similar effect could also reduce our sensitivity to O^+ if atomic O proves very hot and highly dispersed, which could occur if the main source mechanism for lunar O is sputtering or molecular dissociation.

[22] After applying all of these constraints, we identify a sample of 100 individual pickup ion observations, with each observation consisting of a single measurement of the three-dimensional ion distribution by the ESA instrument. Given the typical ESA survey mode cadence of a few minutes, some events have only a few individual observations. The time period shown in Figures 1–2 has 38 between the two probes (by far the most of any single time period). We display the location of these observations in Figure 5. Though we do not pre-apply the following selection criteria, we find that the vast majority of these events occur for times when the magnetic field lies within 25 degrees of perpendicular to the orbit plane, the electric field points toward the probe from the Moon, the flow velocity exceeds 200 km/s, the density exceeds 0.5 cm^{-3}, the spacecraft lies in a wedge from slightly forward of the Moon to 45 degrees behind it, and the predicted pickup ion energy per charge $E*Y_P$ lies between the maximum reflected proton energy/charge of 9 times the solar wind value and the 25 keV/q upper end of the ESA range. Accordingly, we collate all the times that meet these criteria, and show them in Figure 5 as a control sample. The actual observations fill a narrower wedge than the locations/times at which we could in principle see ions, suggesting that a relatively narrow range of ion species may contribute to the identified observations.

[23] We also show the same observations in normalized coordinates, with velocity vectors, along with sample orbits for several masses for comparison, in Figure 6. As for the event in Figures 1–2, we note that most of the pickup ion observations appear consistent with a narrow mass range of ~20–40 amu, though for many we cannot rule out higher masses, given the broad angular response of the instrument. On the other hand, very few observations appear visually consistent with an ion mass below about 20 amu. For the lowest few mass numbers, this may result partly from our selection criteria, as described above. However, we still might expect to observe even ions as light as He^+ near the peak of their cycloidal motion.

5. Inferred Distribution of Lunar Pickup Ion Species and Source Locations

[24] To quantify the ion masses that ARTEMIS could have observed for these 100 pickup ion events, we repeat the same analytical trajectory analysis described in section 3 to find the range of masses that could reach the spacecraft at the

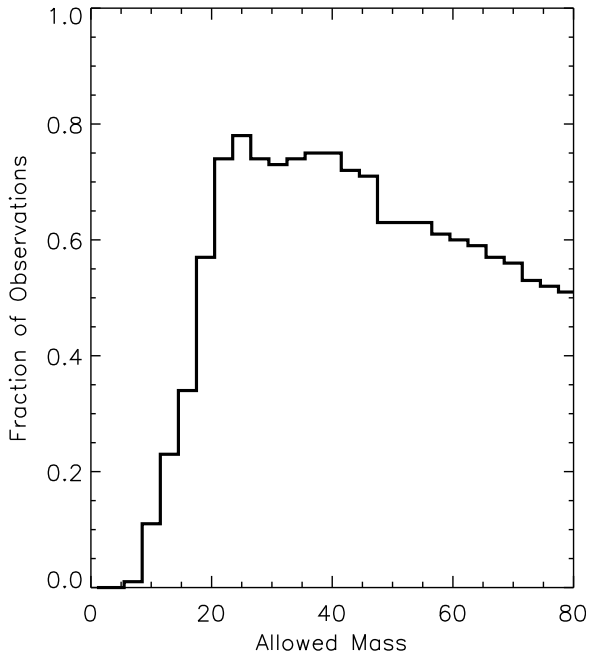

Figure 7. The solid black histogram shows the fraction of the 100 individual ARTEMIS pickup ion observations consistent with each ion mass, taking into account all constraints from trajectory reconstruction and instrument response. The removal of proton contamination also removes virtually all H_2^+ signals and a significant fraction of He^+ signals, but does not significantly reduce sensitivity to higher-mass ions.

correct location, in the correct energy/angle bin, for each observation. We show the results in cumulative form in Figure 7. No single mass can explain all our observations, indicating that ARTEMIS observes multiple ion species. The largest fraction of our observations, 70–80%, are consistent with a mass range of ~20–45 amu. The curve extends to relatively high masses at significant ~50% levels, since for many cases with high mass ions at lower gyrophases we can achieve very little mass-discrimination using angular considerations. On the other hand, very few of our pickup ion observations could have significant contributions from masses below ~15. As discussed in Section 4, several factors may conspire to reduce (but not eliminate) our sensitivity to He^+, but we should have relatively good sensitivity to masses above this. Only about 35% of the observed ions could have masses below ~20 amu, indicating that O^+ cannot comprise a dominant fraction of the observed ions (unless the neutral source has highly non-thermal characteristics). This contrasts with more distant Wind observations, which found a dominant O^+ component [*Mall et al.*, 1998].

[25] We cannot say more with any certainty about the pickup ion species, beyond the curve shown in Figure 7. However, by making some reasonable assumptions, we can converge on a narrower distribution of masses, which though not definite, has plausible characteristics. First, we note that the observations roughly separate into two groups, of which the P1 and P2 observations shown in Figures 3 and 4 provide type examples. The first case, as typified by the P1 example, provides a relatively tight constraint on ion mass, and indicates relatively low starting altitudes. The second case, as typified by the P2 example, provides few constraints on mass, with the possible range extending to high masses, covering a broad range of possible starting altitudes.

[26] We divide the observations into these two groups, and first consider the well-constrained population that satisfy the constraint of $\sigma M/\langle M\rangle < 0.25$ (where $\langle M\rangle$ and σM are the mean and standard deviation of the allowed range of masses). For this population, we make the reasonable assumption that the peak flux for each observation comes solely from the mass for which the trajectory with the peak energy response originates at the lowest altitude. This should prove true on average for both sputtered (zero starting altitude) and exospheric sources (higher neutral density closer to surface). This assumption results in the green mass histogram in Figure 8 (left), containing only the well-constrained cases. As an alternative, we construct a similar green mass histogram in Figure 8 (right) through much the same method, but in this case we equally weight all masses for which the trajectory with the peak energy response originated below 50 km (if, for a given observation, no trajectories originated below 50 km, we take the minimum altitude trajectory as above). Since the predicted neutral density for many exospheric species does not fall off steeply from the surface to ~50 km altitude [*Sarantos et al.*, 2012], we might expect to have a similar response to all species with starting altitudes in this range. Therefore, assuming we have significant contributions from multiple ion species, Figure 8 (right) may provide a somewhat more unbiased estimate. In any case, the two methods result in quite similar spectra, indicating that our result does not depend too strongly on the algorithm.

[27] To build up a plausible mass spectrum for all of our observations, both well-constrained and otherwise, we take the remaining poorly constrained observations, and make the assumption that the mass distribution of each individual poorly constrained observation corresponds to that of the well-constrained cases, over the mass range allowed for the poorly constrained observation (even the poorly constrained cases have some constraints). We then distribute each poorly constrained observation over its allowed mass range according to the portion of the well-constrained histogram (green curve) that covers that mass range. In other words, for each poorly constrained data point, we take the portion of the green histogram that covers the mass range allowed for that data point, and use that portion of the distribution to construct a probability distribution for that data point, such that the total of the weighted probability thus calculated sums to a total of one. After performing this fractional redistribution for each data point, and summing the results, we arrive at a second mass histogram (blue curve). We then sum these two histograms together to form a net histogram (red curve).

[28] We emphasize that we have not actually measured the cumulative mass histograms in Figure 8. The only thing we know with certainty is the distribution of allowed masses in Figure 7. However, by making two reasonable assumptions, we have arrived at a more constrained mass histogram, with some very plausible properties. This favored spectrum has clear peaks at masses of ~20–24 amu, and masses of ~36–40 amu, which correspond directly to the masses for the alkalis Na^+ (23) and K^+ (39). Given that these ions have predicted densities at altitude comparable to or greater than other species in this range [*Sarantos et al.*, 2012], and photo-

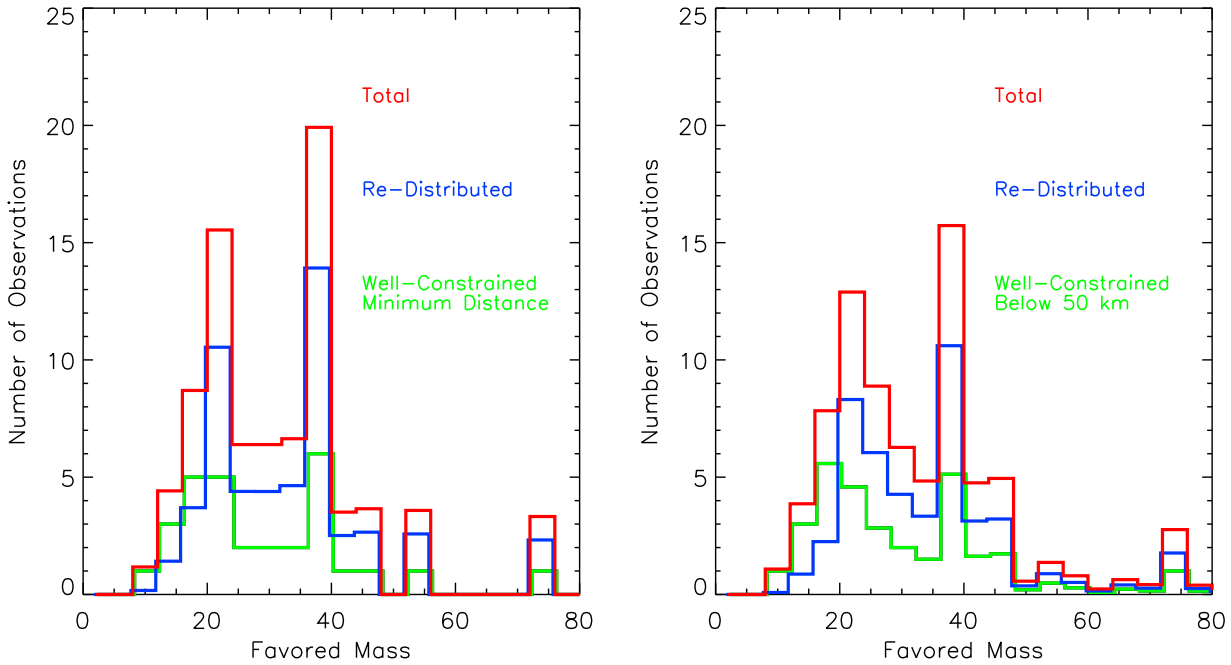

Figure 8. Favored cumulative mass histograms for 100 ARTEMIS pickup ion observations, derived from the assumption the source density should peak at low altitude. The green histograms include all observations with a good constraint on ion mass ($\sigma M/\langle M \rangle < 0.25$). (left) We place each data point at the mass corresponding to the trajectory of peak energy response with the lowest allowed starting altitude for that observation to arrive at the green histogram. (right) We construct the green histogram in a similar fashion, but if more than one mass corresponds to a trajectory of peak energy response with a starting altitude below 50 km, we evenly weight all such masses. The blue histograms in both panels use the probability distribution from the well-constrained points to weight the allowed range of masses for each of the rest of the less well-constrained observations. The red histograms show the resulting cumulative mass distributions. It is not clear yet if these histograms reflect relative abundance.

ionization rates two orders of magnitude larger than other known species in this range [*Huebner et al.*, 1992], these species appear very plausible as an important component of lunar pickup ion observations. On the other hand, Mg^+, Ar^+ and Ca^+ also lie in these mass ranges, and we cannot rule them out, especially if direct ion sputtering dominates over photo-ionization of neutrals.

[29] Finally, as an additional exercise, we take the range of possible source locations corresponding to each point in the histograms of Figure 8 (left), and distribute them in the same fashion as in the construction of that curve to find a distribution of inferred source locations in Figure 9. This source distribution has only as much validity as the mass histogram in Figure 8, and is subject to all the same assumptions and caveats. Despite these limitations, we again arrive at a plausible result. The raw occurrence rate (Figure 9, top) peaks near the surface, and extends broadly above the sunlit hemisphere, consistent with photo-ionization of an exospheric source. Assuming that the probability of observing a given source region scales with the total source volume of the cylindrical element represented in the 2-d plot, as it roughly should, Figure 9 (bottom) provides a less biased map of the pickup ion source occurrence. This inferred source map could plausibly correspond to photo-ionization of an exospheric source with a scale height on the order of ~1000 km, with the enhanced contribution from near the surface possibly indicating smaller scale height or the direct sputtering of ions from the surface. The inferred source appears to exhibit a dependence on solar zenith angle as expected for either directly sputtered ions or ionized neutral exospheric constituents. A secondary spot at low altitudes near the terminator could represent a contribution from Ar^+.

6. Correlation of Pickup Ion Observations With External Drivers

[30] As we noted in section 4, we do not observe pickup ions at all the times and locations for which favorable conditions exist. Partly, as Figure 5 suggests, this may reflect a spatial constraint related to a relatively limited range of pickup ion masses. However, it could also indicate that some solar wind and/or illumination conditions lead to an increased chance of observing pickup ions, or to a higher flux of pickup ions. We consider this possibility in this final section.

[31] First, we investigate whether lunar phase may affect the probability of observing pickup ions, by plotting the distribution of the phase (the phi angle of the Moon in GSE coordinates) for all the observations in Figure 10. We find an increased number of observations before and after full Moon, and a complete dropout around full Moon; however, these trends also exist in the distribution of favorable conditions for pickup ion observation by ARTEMIS. Indeed, the chance of observing pickup ions appears statistically uniform when normalized by the number of opportunities. The

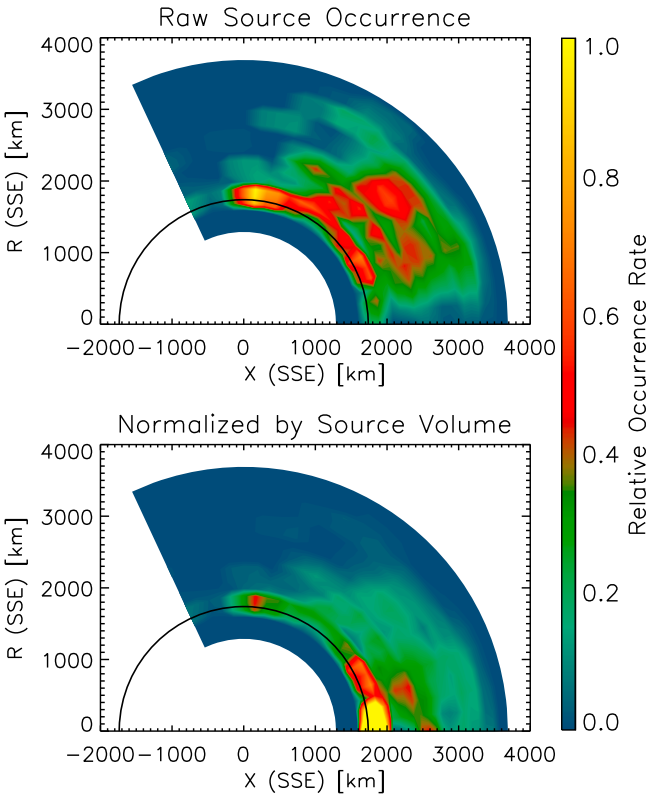

Figure 9. Favored source location corresponding to the favored mass distribution of Figure 8 (left), in cylindrical coordinates. (top) Raw occurrence; and (bottom) occurrence normalized by spatial volume.

increase in observation opportunities before and after full Moon has no clear cause, but represents only a few days and may therefore prove completely random. The highest peak in observations at phase −150 corresponds to the 38 observations from P1 and P2 from the single event of Figures 1–2, which occurred during a particularly long period of favorable observation conditions. Finally, the dropout around full Moon corresponds to the period in which the Moon lies inside the Earth's magnetosphere, with no prevailing flow or convection electric field strong enough to accelerate any lunar ions that may exist into an energetic plume that our event selection would have identified.

[32] As a final exercise, we investigate whether solar illumination or solar wind proton flux affect either the probability of seeing pickup ions, or the flux of pickup ions seen by ARTEMIS. We do not consider a third element that could control pickup ion fluxes, namely micrometeorite flux [*Smith et al.*, 1999]; however, we have noted no obvious correlation between pickup ion observations and known meteor streams. For solar wind proton flux, we use the ARTEMIS ESA measurements. For solar illumination, we use the TIMED / SEE Lyman α composite [*Woods et al.*, 2000a, 2000b] as a proxy. In Figure 11, we show the distribution of these two quantities for all data during the time period from 9/15/2011–2/5/2012, for times with favorable conditions for pickup ion observations (as previously defined), and for 29 pickup ion events. To obtain the most unbiased statistical distribution, we opt to consider groups of observations that occur sequentially as a single event. For our purposes, an event is defined as a separate hour during which ARTEMIS observed pickup ions. Some events, such as those shown in Figures 1–2, have many observations, while others have only a few.

[33] Figure 11 shows no significant differences in the solar wind flux for times when ARTEMIS observes pickup ions. For Lyman α flux, we see a small trend toward increased probability of observing pickup ions at times with higher photon flux, but the trend has little statistical significance given the small number of events. Apparently, enhanced solar wind flux or solar photon flux do not significantly increase the probability that ARTEMIS will observe ions. This seems somewhat surprising, given that sputtering and photo-ionization, the two main expected source processes for pickup ions, depend on these two inputs. This may indicate that lunar pickup ions always exist around the Moon at some level, and the chance of ARTEMIS observing them depends purely on geometrical considerations. Figure 5, which shows that all of the ARTEMIS observations lie in a narrow spatial region, provides some support for this hypothesis.

[34] We can also investigate whether the flux of pickup ions (when observed) depends on either of these parameters. As above, we separate our observations into 29 events, and calculate the average pickup ion differential energy flux observed by the ESA instrument during each event. For most observations, which lie in a single ESA energy bin, differential energy flux is directly proportional to total number flux. We show the results as a function of solar wind proton and solar photon flux, using the same data sets as above, in Figure 12. We find that the pickup ion differential energy flux correlates with solar wind flux, and anti-correlates with photon flux.

[35] The significant correlation between pickup ion flux and solar wind flux clearly suggests that charged particle

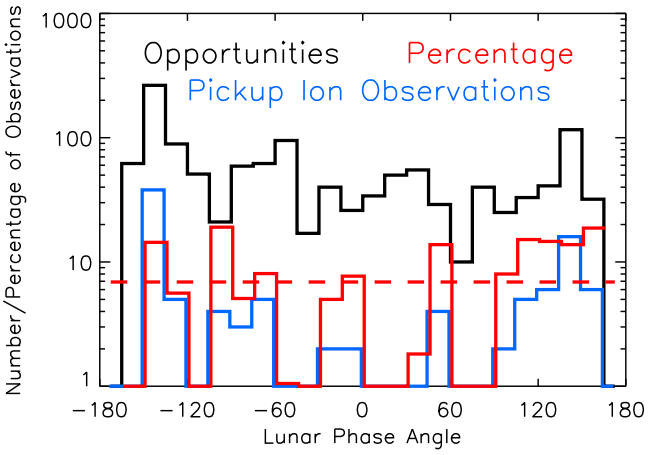

Figure 10. Distribution of pickup ion observations for the time period of September 15th, 2011 through February 5th, 2012 as a function of lunar phase angle (defined as the phi angle of the Moon in GSE coordinates, with +/−180 = full moon, 0 = new moon), as compared to the distribution of favorable conditions (defined in the same way as Figure 5, as described in the text). The red curve shows the percentage of times with favorable conditions during which ARTEMIS observed pickup ions, and the dashed red line shows the average percentage.

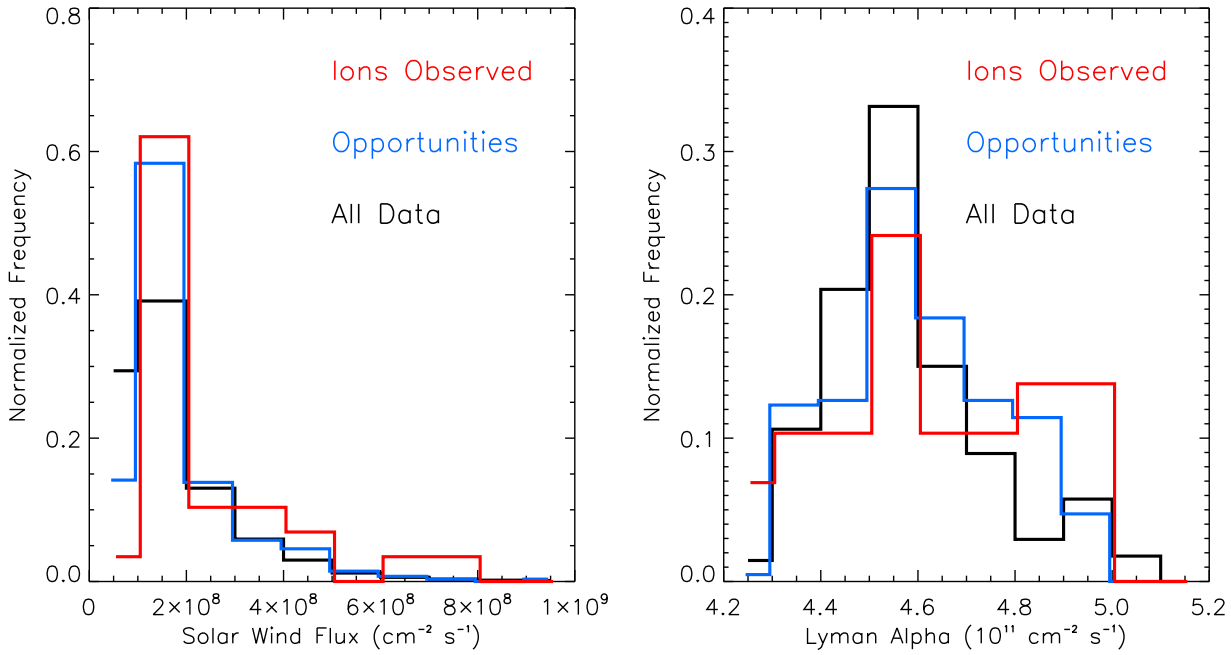

Figure 11. Frequency distributions of solar wind proton and Lyman α photon flux for all times between September 15th, 2011 and February 5th, 2012, for times in that range favorable for pickup ion observations, and for the 29 ARTEMIS pickup ion events in that time period. Many events include multiple individual observations, but we count these as a single event for the purposes of this statistical analysis unless the observations span more than one hour.

sputtering controls pickup ion fluxes. However, we cannot determine whether this indicates direct sputtering of ions from the surface, or sputtering of neutrals that rapidly become ionized once in the exosphere. Direct sputtering of ions from the surface provides the simpler hypothesis. The possible control of the exosphere by sputtering is difficult to ascertain, but many refractory elements from the surface (e.g., Al, Si) may be promoted to the gas phase by

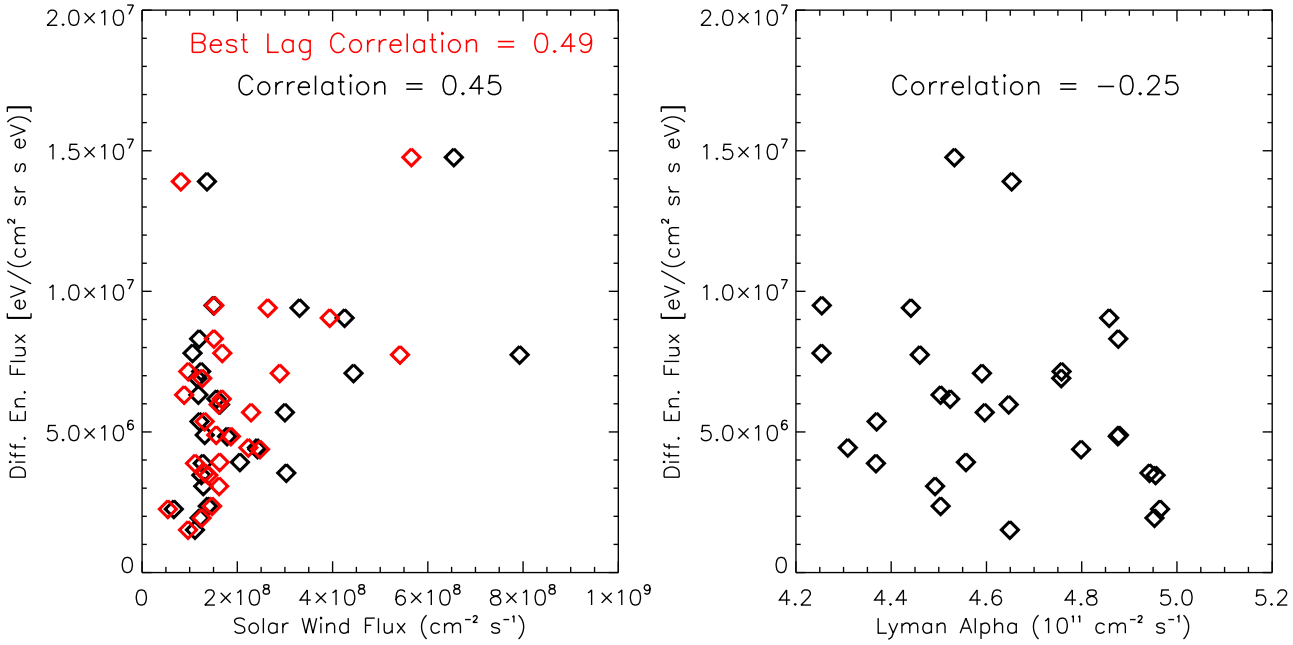

Figure 12. Scatterplots of observed average pickup ion differential energy flux versus solar wind proton and Lyman α photon flux, for the 29 ARTEMIS pickup ion events of Figure 11. Red points in the left panel show the same events, but with a lag of 30 min between solar wind flux and pickup ion differential energy flux.

impacts and sputtering in equal amounts [*Sarantos et al.*, 2012]. The lifetime of even the neutral species with the highest photo-ionization rates is a substantial fraction of a day, suggesting that if the exosphere consisted of significant amounts of sputtered neutrals, then we might expect some time lag between the solar wind flux input and the pickup ion signal. We checked various time lags, and found the best (though only very slightly better) correlation for a time lag of 30 min between solar wind input and pickup ion output. This lag is short compared to most neutral lifetimes, suggesting that if indirect sputtering dominates, the process of pickup ion release must be source-limited, rather than process-limited. This would suggest that sufficient photon input always exists to rapidly ionize ions, but this can only occur when a sufficient neutral source population exists.

[36] Meanwhile, the weak or slightly negative correlation observed with photon flux proves somewhat difficult to explain, if photo-ionization of exospheric neutrals plays a significant role. Possibly, photon-stimulated desorption from the surface competes with sputtering. If so, high photon flux might remove the surface source population faster than sputtering, leading to a reduction in sputtered flux during periods with high photon flux. This again would point to a source-limited process. This might also argue for direct sputtering as the dominant producer of ions, rather than subsequent ionization of sputtered neutrals, since photo-desorbed neutrals should ionize just as sputtered neutrals do.

[37] Given the moderate correlation coefficients found in both cases, any real correlation probably only applies to a subset of the events. Therefore, we clearly must allow for the possibility that more than one process operates (as we should expect given what we know about the lunar environment), leading to competing factors that control the release of pickup ions.

7. Implications

[38] ARTEMIS observations show that pickup ions commonly exist in the lunar environment. When background plasma conditions favor the observation of pickup ions in an equatorial orbit, ARTEMIS observes such ions ~7% of the time. All of these observations cluster in a narrow region (see Figures 5–6), suggesting that ARTEMIS observes a relatively narrow range of species, and that the true occurrence rate may actually prove much higher than 7%, taking into account spatial constraints related to the pickup ion trajectories.

[39] Though the ESA ion instrument has no mass resolution capability, we can constrain the range of the observed ion species by taking advantage of the fact that pickup ions follow an easily analytically described trajectory, forming a narrow beam in both energy and angle. Utilizing all available constraints, we find that most of the ARTEMIS ion observations are consistent with masses in the range of ~20–45 amu, and that a smaller percentage could have higher or lower masses, but only a very small percentage could have masses below ~15 amu (see Figure 7). No single mass can explain all observations, so the observations must contain multiple ion species. Given the many expected ion species around the Moon (Table 1), this conclusion should be unsurprising.

[40] The above is all we can state with certainty about the distribution of pickup ion species. If, however, we make the assumption that the peak flux should come from lower altitudes, and consider only those observations with a relatively well-constrained mass range, we can arrive at a favored mass spectrum (green curves in Figure 8) with peaks at masses 16–24 and 36–40 amu. If the less well-constrained observations, which tend to have higher inferred starting altitudes, also have the same mass distribution over the allowed ranges, the full resulting spectrum has narrow peaks at masses 20–24 and 36–40 amu. These masses are consistent with Na^+, Mg^+, K^+, Ar^+, and Ca^+. If the assumptions that go into constructing this narrower spectrum do not hold for all observations, other ions in the mass range of ~20–45 amu, such as Al^+ and Si^+, could also play an important role. Surprisingly, the ARTEMIS observations indicate that He^+ and O^+ do not comprise a significant fraction of the observations. As discussed, we may have somewhat reduced sensitivity to He^+, but should still observe it near the peak of its cycloidal motion.

[41] Other features of the distribution of observations may help narrow the plausible ion species. We find that the pickup ion flux has a good correlation with solar wind proton flux, but no correlation (in fact a slight anti-correlation) with photon flux. Therefore, sputtering (or perhaps ion-enhanced photo-stimulated desorption of neutrals) must play a key role in either directly producing ions from the surface, or producing neutrals that subsequently become ionized. The lack of a correlation with photon flux suggests a source-limited release of ions.

[42] Finally, we found that many observations had a plausible source near the surface, but that many others appeared inconsistent with a near-surface source for any reasonable ion mass. Therefore, at least some of the observed ions must have an exospheric source. Given that exospheric Na and K have fairly substantial neutral column densities, as well as photo-ionization rates two orders of magnitude greater than other species in the same mass range, we might suspect that these two species may form an important component of the observed pickup ion plumes. At the same time, sputtering experiments indicate that sputtered Mg, Na, Al, Si, and K all have a very high percentage of ions in the released gases [*Elphic et al.*, 1991; *Dukes et al.*, 2011]. Therefore, any of these ions could plausibly contribute to the fraction of our observations consistent with release at the surface. The inferred source distribution, a highly derived product (Figure 9), exhibited a dependence on solar zenith angle, consistent with either direct sputtering of ions or with photo-ionization of an exospheric source.

[43] Much work remains to be done before we can reach stronger conclusions as to the exact species and release mechanism. More ARTEMIS observations become available every day, and eventually we should have a data set large enough to split into distinct samples, to more carefully address ions with different apparent source altitudes, and ions with different apparent source mechanisms as suggested by correlation or lack thereof with various external drivers. We also anticipate making further progress by comparing with the detailed model predictions now becoming available [*Hartle et al.*, 2011; *Sarantos et al.*, 2012].

[44] **Acknowledgments.** We thank NASA's Lunar Science institute for supporting this work, and acknowledge NASA contract NAS5-02099 for THEMIS/ARTEMIS support. We thank K.-H. Glassmeier and U. Auster for the use of FGM data provided under the lead of the Technical University of Braunschweig and with financial support through the German Ministry

for Economy and Technology and the German Center for Aviation and Space (DLR) under contract 50 OC 0302. We thank the Laboratory for Atmospheric and Space Physics for providing TIMED/SEE data.

References

Angelopoulos, V. (2011), The ARTEMIS mission, *Space Sci. Rev.*, *165*, 3–25, doi:10.1007/s11214-010-9687-2.

Auster, H. U., et al. (2008), The THEMIS fluxgate magnetometer, *Space Sci. Rev.*, *141*, 235–264, doi:10.1007/s11214-008-9365-9.

Cladis, J. B., W. E. Francis, and R. R. Vondrak (1994), Transport toward Earth of ions sputtered from the Moon's surface by the solar wind, *J. Geophys. Res.*, *99*, 53–64, doi:10.1029/93JA02672.

Dukes, C. A., W. Y. Chang, M. Fama, and R. A. Baragiola (2011), Laboratory studies on the sputtering contribution to the sodium atmospheres of Mercury and the Moon, *Icarus*, *212*, 463–469, doi:10.1016/j.icarus.2011.01.027.

Elphic, R. C., H. O. Funsten, B. L. Barraclough, D. J. McComas, M. T. Paffett, D. T. Vaniman, and G. Heiken (1991), Lunar surface composition and solar wind-induced secondary ion mass spectrometry, *Geophys. Res. Lett.*, *18*, 2165–2168, doi:10.1029/91GL02669.

Fastie, W. G., P. D. Feldman, R. C. Henry, H. W. Moos, C. A. Barth, G. E. Thomas, and T. M. Donahue (1973), A search for far-ultraviolet emissions from the lunar atmosphere, *Science*, *182*, 710–711, doi:10.1126/science.182.4113.710.

Feldman, P. D., and D. Morrison (1991), The Apollo 17 ultraviolet spectrometer: Lunar atmosphere measurements revisited, *Geophys. Res. Lett.*, *18*, 2105–2109, doi:10.1029/91GL01998.

Flynn, B. C., and S. A. Stern (1996), A spectroscopic survey of metallic species abundances in the lunar atmosphere, *Icarus*, *124*, 530–536, doi:10.1006/icar.1996.0228.

Freeman, J. W., Jr., and J. L. Benson (1977), A search for gaseous emissions from the Moon, *Phys. Earth Planet. Inter.*, *14*, 276–281, doi:10.1016/0031-9201(77)90177-7.

Halekas, J. S., Y. Saito, G. T. Delory, and W. M. Farrell (2011), New views of the lunar plasma environment, *Planet. Space Sci.*, *59*, 1681–1694, doi:10.1016/j.pss.2010.08.011.

Hartle, R. E., and R. M. Killen (2006), Measuring pickup ions to characterize the surfaces and exospheres of planetary bodies: Applications to the Moon, *Geophys. Res. Lett.*, *33*, L05201, doi:10.1029/2005GL024520.

Hartle, R. E., M. Sarantos, and E. C. Sittler Jr. (2011), Pickup ion distributions from three-dimensional neutral exospheres, *J. Geophys. Res.*, *116*, A10101, doi:10.1029/2011JA016859.

Hilchenbach, M., D. Hovestadt, B. Klecker, and E. Mobius (1991), Detection of singly ionized energetic lunar pick-up ions upstream of Earth's bow shock, in *Solar Wind Seven*, edited by E. Marsch and G. Schwenn, pp. 150–155, Pergamon, New York.

Hilchenbach, M., D. Hovestadt, B. Klecker, and E. Mobius (1993), Observation of energetic lunar pick-up ions near Earth, *Adv. Space Res.*, *13*, 321–324, doi:10.1016/0273-1177(93)90086-Q.

Hodges, R. R., Jr. (1976), The escape of solar-wind carbon from the moon, *Proc. Lunar Sci. Conf.*, *7th*, 493–500.

Hoffman, J. H., and R. R. Hodges Jr. (1975), Molecular gas species in the lunar atmosphere, *Moon*, *14*, 159–167, doi:10.1007/BF00562981.

Hoffman, J. H., R. R. Hodges Jr., and D. E. Evans (1973), Lunar atmospheric composition results from Apollo 17, *Proc. Lunar Sci. Conf.*, *4th*, 2865–2875.

Huebner, W. F., J. J. Keady, and S. P. Lyon (1992), Solar photo rates for planetary atmospheres and atmospheric pollutants, *Astrophys. Space Sci.*, *195*, 1–294, doi:10.1007/BF00644558.

Killen, R. M., D. M. Hurley, and W. M. Farrell (2012), The effect on the lunar exosphere of a coronal mass ejection passage, *J. Geophys. Res.*, *117*, E00K02, doi:10.1029/2011JE004011.

Lue, C., Y. Futaana, S. Barabash, M. Wieser, M. Holmstrom, A. Bhardwaj, M. B. Dhanya, and P. Wurz (2011), Strong influence of lunar crustal fields on the solar wind flow, *Geophys. Res. Lett.*, *38*, L03202, doi:10.1029/2010GL046215.

Mall, U., E. Kirsch, K. Cierpka, B. Wilken, A. Soding, F. Neubauer, G. Gloeckler, and A. Galvin (1998), Direct observation of lunar pick-up ions near the Moon, *Geophys. Res. Lett.*, *25*, 3799–3802, doi:10.1029/1998GL900003.

McFadden, J. P., C. W. Carlson, D. Larson, M. Ludlam, R. Abiad, B. Elliott, P. Turin, M. Marckwordt, and V. Angelopoulos (2008a), The THEMIS ESA plasma instrument and in-flight calibration, *Space Sci. Rev.*, *141*, 277–302, doi:10.1007/s11214-008-9440-2.

McFadden, J. P., C. W. Carlson, D. Larson, J. Bonnell, F. Mozer, V. Angelopoulos, K.-H. Glassmeier, and U. Auster (2008b), THEMIS ESA first science results and performance issues, *Space Sci. Rev.*, *141*, 477–508, doi:10.1007/s11214-008-9433-1.

Mendillo, M., J. Baumgardner, and B. Flynn (1991), Imaging observations of the extended sodium atmosphere on the Moon, *Geophys. Res. Lett.*, *18*, 2097–2100, doi:10.1029/91GL02622.

Potter, A. E., and T. H. Morgan (1988), Discovery of sodium and potassium vapor in the atmosphere of the Moon, *Science*, *241*, 675–680, doi:10.1126/science.241.4866.675.

Saito, Y., et al. (2008), Solar wind proton reflection at the lunar surface: Low energy ion measurements by MAP-PACE onboard SELENE (KAGUYA), *Geophys. Res. Lett.*, *35*, L24205, doi:10.1029/2008GL036077.

Sarantos, M., R. Killen, A. Sharma, and J. A. Slavin (2010), Sources of sodium in the lunar exosphere: Modeling using ground-based observations of sodium emission and spacecraft data of the plasma, *Icarus*, *205*, 364–374, doi:10.1016/j.icarus.2009.07.039.

Sarantos, M., R. M. Killen, D. A. Glenar, M. Benna, and T. J. Stubbs (2012), Metallic species, oxygen and silicon in the lunar exosphere: Upper limits and prospects for LADEE measurements, *J. Geophys. Res.*, *117*, A03103, doi:10.1029/2011JA017044.

Smith, S. M., J. K. Wilson, J. Baumgardner, and M. Mendillo (1999), Discovery of the distant lunar sodium tail and its enhancement following the Leonid meteor shower of 1998, *Geophys. Res. Lett.*, *26*, 1649–1652, doi:10.1029/1999GL900314.

Stern, S. A. (1999), The lunar atmosphere: History, status, current problems, and context, *Rev. Geophys.*, *37*, 453–491, doi:10.1029/1999RG900005.

Stern, S. A., and B. C. Flynn (1995), Narrow-field imaging of the lunar sodium exosphere, *Astron. J.*, *109*, 835–841, doi:10.1086/117327.

Stern, S. A., J. W. Parker, T. H. Morgan, B. C. Flynn, D. M. Hunten, A. L. Sprague, M. Mendillo, and M. C. Festou (1997), An HST search for magnesium in the lunar atmosphere, *Icarus*, *127*, 523–526, doi:10.1006/icar.1997.5716.

Tanaka, T., et al. (2009), First in situ observation of the Moon-originating ions in the Earth's magnetosphere by MAP-PACE on SELENE (KAGUYA), *Geophys. Res. Lett.*, *36*, L22106, doi:10.1029/2009GL040682.

Vondrak, R. R., J. W. Freeman, and R. A. Lindeman (1974), Measurements of lunar atmospheric loss rate, *Proc. Lunar Sci. Conf.*, *5th*, 2945–2954.

Wang, X. D., et al. (2011), Detection of m/q = 2 pickup ions in the plasma environment of the Moon: The trace of exospheric H2+, *Geophys. Res. Lett.*, *38*, L14204, doi:10.1029/2011GL047488.

Woods, T. N., K. Tobiska, G. J. Rottman, and J. R. Worden (2000a), Improved solar Lyman α irradiance modeling from 1947 through 1999 based on UARS observations, *J. Geophys. Res.*, *105*, 27,195–27,215, doi:10.1029/2000JA000051.

Woods, T. N., et al. (2000b), The TIMED solar EUV experiment, *Phys. Chem. Earth Part C*, *25*(5–6), 393–396, doi:10.1016/S1464-1917(00)00040-4.

Yokota, S., and Y. Saito (2005), Estimation of picked-up lunar ions for future compositional remote SIMS analyses of the lunar surface, *Earth Planets Space*, *57*, 281–289.

Yokota, S., et al. (2009), First direct detection of ions originating from the Moon by MAP-PACE IMA onboard SELENE (KAGUYA), *Geophys. Res. Lett.*, *36*, L11201, doi:10.1029/2009GL038185.